Journal of
Chemical Engineering & Process Technology

Uchiyama and Yoshii, J Chem Eng Process Technol 2015, 6:4
DOI: 10.4172/2157-7048.1000245

Research Article Open Access

Numerical Study of the Entrainment and Transport of Gas Bubbles by a Vortex Ring

Tomomi Uchiyama[1*] and Yutaro Yoshii[2]

[1]*EcoTopia Science Institute, Nagoya University, Furo-cho, Chikusa-ku, Nagoya 464-8603, Japan*
[2]*Software Cradle Co., Ltd, 3-4-5, Umeda, Kita-ku, Osaka 530-0001, Japan*

Abstract

The control of the motion of small gas bubbles by a vortex ring is explored through numerical simulation. Hydrogen bubbles with a diameter of 0.2 mm are arranged in quiescent water, forming a bubble cluster. A vortex ring is launched vertically, passing through the bubble cluster. The behaviors of the vortex ring and bubble motion are analyzed. The diameter of the vortex ring at launch is 42.5 mm, and the bubble volume fraction is less than 0.04. As the vortex ring convects through the bubble cluster, it displaces and entrains the bubbles. After the vortex ring passes through the cluster, the bubbles are involved in the vortex ring. The research also clarifies the evolution of the diameter and circulation of the vortex ring.

Keywords: Multiphase flow; Numerical simulation; Bubble; Vortex ring; Entrainment

Introduction

Gas-liquid bubbly two-phase flows are observed in various engineering applications such as chemical reactors, waste treatment systems, and heat exchangers. Numerous previous studies have clarified the flow characteristics, such as the turbulent structure and the phase distribution of bubbly flows [1-3]. Moreover, because bubble motion is an important and elementary phenomenon governing a bubbly flow, there have been attempts to control this motion using an ultrasonic wave [4,5] and a swirling flow in a circular pipe [6,7]. However, the ultrasonic wave method is limited to a single bubble, and the swirling flow method cannot accurately control bubble motion.

When water is ejected from a cylinder into quiescent water, a vortex core forming a closed circle occurs. Such a vortex ring undergoes self-induced convection in a direction perpendicular to the plane of the circle. Small gas bubbles in a liquid flow preferentially distribute around the high-vorticity region [8,9]. By noting that the vorticity is highly concentrated on the vortex core of the vortex ring, one of the authors [10] conducted an experimental study on the behavior of a vortex ring in bubbly mixtures. Small hydrogen bubbles were generated by water electrolysis at the bottom of a water tank. The buoyancy of the bubbles forced them to rise, creating a bubble plume. A vortex ring was launched vertically upward into the bubble plume from a cylinder mounted at the tank bottom. The bubbles became entrained in the vortex core and changed the convection of the vortex ring, demonstrating that a vortex ring can be successfully employed to control bubble motion and to entrain and transport bubbles if the strength and scale of the vortex ring are set appropriately. Active bubble motion control is a technology with applications in the drive, supply, and removal of bubbles dispersed in a liquid. It can be utilized in various engineering contexts such as the control of chemical reactions and heat transfer. Yet, there are only few studies on the interaction between a vortex ring and bubbles, besides the experimental works of Sridhar-Katz [11,12] and no attempts have been made to apply this approach to bubble motion control.

The vortex in cell (VIC) method is a numerical method for simulating incompressible flows. It discretizes the vorticity field into vortex elements and computes the time evolution of the flow by tracing the convection of each vortex element using a Lagrangian approach. The Lagrangian method markedly reduces numerical diffusion and improves numerical stability. The authors [13] previously proposed two improvements to the VIC method. First, a staggered-grid discretization method guarantees consistency among discretized equations and prevents numerical oscillations in a solution. Second, a correction method for the vorticity enables the computation of vorticity fields to satisfy the solenoidal condition. The improved VIC method was applied to the direct numerical simulation (DNS) of a turbulent channel flow [13]. The DNS successfully captured organized flow structures such as streaks and streamwise vortices in the near-wall region, demonstrating that the VIC method is applicable to the DNS of wall turbulent flows. The authors [14] also presented a simulation method for a bubbly flow using the VIC method. The behaviors of the vortex element and bubble motion are simultaneously analyzed by the Lagrangian method. The proposed method was applied to the simulation of a bubble plume in a water tank to demonstrate its validity [14]. Small air bubbles were released successively from the base of the tank, and their rise induced a bubble plume. The simulated bubble behavior and water velocity were favorably compared with the existing results. The proposed method was also used for the simulation of an air-water bubbly jet issued vertically upward from a nozzle of a square-cross section [15]. The Reynolds number of water is 5000, the bubble diameter is 0.2 mm, and the bubble volumetric flow rate is 0.0025. The simulated results such as the water momentum diffusion in the lateral direction were shown to agree with measured data.

This study aims to investigate the control of the motion of small gas bubbles by a vortex ring through numerical simulation. Small hydrogen bubbles are arranged in quiescent water, and a vortex ring is launched toward the bubble cluster. The behaviors of the vortex ring and bubble motion are analyzed by the VIC method used in a previous

***Corresponding author:** Tomomi Uchiyama, EcoTopia Science Institute, Nagoya University, Furo-cho, Chikusa-ku, Nagoya 464-8603, Japan, Tel: 8152789-5187; E-mail: uchiyama@is.nagoya-u.ac.jp

Received September 08, 2015; **Accepted** September 21, 2015; **Published** September 30, 2015

Citation: Uchiyama T, Yoshii Y (2015) Numerical Study of the Entrainment and Transport of Gas Bubbles by a Vortex Ring. J Chem Eng Process Technol 6: 245. doi:10.4172/2157-7048.1000245

study [14]. The simulation demonstrates that the vortex ring convects through the bubble cluster, displacing and entraining the bubbles, and that the bubbles are involved in the vortex ring after passing through the cluster. The simulation also clarifies changes in the diameter and circulation of the vortex ring.

Basic Equations

Assumptions

Assumptions employed in the simulation are as follows:

(a) The mixture is a gas-liquid bubbly flow with entrained small bubbles.

(b) Both phases are incompressible, and no phase change occurs.

(c) The mass and momentum of the gas-phase are negligible compared with those of the liquid-phase.

(d) The bubbles maintain their spherical shape with neither fragmentation nor coalescence.

Governing equations of bubbly flow

Under assumptions (a), (b), and (c), mass and momentum conservation equations for two-phase mixtures are expressed as follows:

$$\frac{\partial \alpha_l}{\partial t} + \nabla \cdot (\alpha_l u_l) = 0 \tag{1}$$

$$\alpha_l \frac{Du_l}{Dt} = -\frac{1}{\rho_l}\nabla p + \nabla \cdot \left[\nu_m \left(\nabla u_l + (\nabla u_l)^T \right) \right] + \alpha_l g \tag{2}$$

where ν_m is the kinematic viscosity considering the gas volume fraction, α_g given by the equation as follows [16]:

$$\nu_m = (1+\alpha_g)\nu_l \tag{3}$$

The volume fractions satisfy the following relation:

$$\alpha_g + \alpha_l = 1 \tag{4}$$

It is postulated that the pressure gradient force, the virtual mass force, the drag force, the gravitational force, and the lift force act on the bubbles. Following assumption (d), the equation of motion for the bubble would therefore be expressed by

$$\frac{du_g}{dt} = \frac{1+C_V}{\beta+C_V}\frac{Du_l}{Dt} - \frac{1}{\beta+C_V}\frac{3C_D}{4d}|u_g-u_l|(u_g-u_l) + \frac{\beta-1}{\beta+C_V}g - \frac{C_L}{\beta+C_V}(u_g-u_l)\times(\nabla\times u_l) \tag{5}$$

where d is the bubble diameter, β is the density ratio ($=\rho_g/\rho_l$).C_V, C_D, and C_L are the virtual mass coefficient, the drag coefficient, and the lift coefficient, respectively. C_D is given by

$$C_D = (24/Re_b)\left(1+0.15Re_b^{0.687}\right) \tag{6}$$

where $Re_b = d|u_g - u_l|/\nu_l$

Vorticity equation and orthogonal decomposition of liquid velocity

Taking the curl of Eq. (2), the vorticity equation for the bubbly flow is derived,

$$\frac{\partial \omega}{\partial t} + \nabla\times(\omega u_l) = \nabla\times(u_l\omega) + \frac{1}{\alpha_l}\nabla\times\nabla\times\left[\nu_m\left(\nabla u_l + (\nabla u_l)^T\right)\right] + \frac{1}{\alpha_l}\nabla\alpha_l\times\left(g - \frac{Du_l}{Dt}\right) \tag{7}$$

Where ω is the vorticity of the liquid-phase.

$$\omega = \nabla \times u_l \tag{8}$$

According to the Helmholtz theorem, any vector field can be represented as the summation of the gradient of a scalar potential ϕ and the curl of a vector potential ψ. Thus, the liquid velocity u_l is written as

$$u_l = \nabla\varphi + \nabla\times\psi \tag{9}$$

The velocity calculated from Eq. (9) remains unaltered when any gradient of a scalar function is added to ψ. To remove this arbitrariness, the following solenoidal condition is imposed on ψ:

$$\nabla\cdot\psi = 0 \tag{10}$$

When substituting Eq. (9) into Eq. (1), we obtain

$$\frac{\partial \alpha_l}{\partial t} + \nabla\cdot\left[\alpha_l(\nabla\varphi + \nabla\times\psi)\right] = 0 \tag{11}$$

Taking the curl of Eq. (9) and substituting Eq. (10) into the resultant equation, the vector Poisson equation for ψ is derived:

$$\nabla^2\psi = -\omega \tag{12}$$

Numerical Method Based on VIC Method

Discretization of vorticity field by vortex element

Once ϕ and ψ are computed from Eqs. (11) And (12) respectively, the velocity u_l is calculated from Eq. (9). The vorticity ψ in Eq. (12) is estimated from Eq. (7). The VIC method discretizes the vorticity field by vortex element and calculates the distribution of ω by tracing the convection of each vortex element.

It is postulated that the position vector and vorticity for the vortex element *p* are $x_p=(x_p,y_p,z_p)$ and ω_p, respectively. The Lagrangian form of the vorticity equation, Eq. (7), is written as

$$\frac{dx_p}{dt} = u_l \tag{13}$$

$$\frac{d\omega_p}{dt} = \nabla\cdot(u_l\omega) + \frac{1}{\alpha_l}\nabla\times\nabla\cdot\left[\nu_m\left(\nabla u_l + (\nabla u_l)^T\right)\right] + \frac{1}{\alpha_l}\nabla\alpha_l\times\left(g - \frac{Du_l}{Dt}\right) \tag{14}$$

When the position and vorticity of a vortex element are known at time t, the values at t+Δt are computed from the Lagrangian calculation of Eqs. (13) and (14). Following the VIC method, the flow field is divided into computational grid cells to define ψ, ϕ and ω on the grids. If ω is defined at a position $\boldsymbol{x}_k = (x_k, y_k, z_k)$, the vorticity ω is assigned to x_k, or a vortex element with vorticity ω is redistributed onto the grid:

$$\omega(x_k) = \sum_p^{N_v} \omega_p W\left(\frac{x_k - x_p}{\Delta x}\right) W\left(\frac{y_k - y_p}{\Delta y}\right) W\left(\frac{z_k - z_p}{\Delta z}\right) \tag{15}$$

where N_v is the number of vortex elements, and Δ_x, Δ_y and Δ_z, are the grid widths. For the redistribution function W, the frequently used equation given below for a single-phase flow simulation [17] is applied:

$$W(\varepsilon) = \begin{cases} 1 - 2.5\varepsilon^2 + 1.5|\varepsilon|^3 & |\varepsilon| < 1 \\ 0.5(2-|\varepsilon|)^2(1-|\varepsilon|) & 1 \le |\varepsilon| \le 2 \\ 0 & |\varepsilon| > 2 \end{cases} \tag{16}$$

Calculation of gas volume fraction

The above mentioned grid cells are also used to calculate the gas volume fraction α_g. It is postulated that a bubble with volume v_r exists at $x_g = (x_g, y_g, z_g)$, the volume fraction α_g on a grid point *q* with position vector $x_q = (x_q, y_q, z_q)$, is given by

$$\alpha_g(x_q) = \sum_r^{N_b} \frac{v_r}{\Delta x\Delta y\Delta z} W_\alpha\left(\frac{x_q - x_g}{\Delta x}\right) W_\alpha\left(\frac{y_q - y_g}{\Delta y}\right) W_\alpha\left(\frac{z_q - z_g}{\Delta z}\right) \tag{17}$$

where N_b is the number of bubbles. For the function W_α, the following redistribution function for vorticity [17] is employed:

$$W_\alpha(\varepsilon)=\begin{cases}0.5(|\varepsilon|+1.5)^2-1.5(|\varepsilon|+0.5)^2 & |\varepsilon|\le 0.5\\ 0.5(-|\varepsilon|+1.5)^2 & 0.5\le|\varepsilon|\le 0.5\\ 0 & |\varepsilon|>1.5\end{cases} \quad (18)$$

Discretization of vorticity field by vortex element

A staggered grid is used to solve Eqs. (11) and (12) so as to ensure consistency between the discretized equations and to prevent numerical oscillations of the solution. Figure 1 shows the grid. The scalar potential ϕ and the gas volume fraction α_g are defined at the center of a grid cell, the liquid velocity u_l is defined at the sides, and the vorticity ω and the vector potential ψ are defined at the edges.

The vorticity field is discretized with vortex element and expressed by the superposition of the vorticity distribution around each vortex element, as found from Eq. (15). Thus, the vorticity field obtained from Eq. (15), denoted by ϖ_r and does not always satisfy the solenoidal condition. The curl of the velocity calculated using results in the vorticity satisfying the solenoidal condition. This correction method is therefore used in the simulation.

Numerical procedure

Given the flow at time t, the flow at t + Δt is simulated by the procedure as follows:

(1) Calculate the bubble motion from Eq. (5).

(2) Calculate α_g from Eq. (17), and compute α_l from Eq. (4).

(3) Calculate the time rate of change for ω at every grid point from Eq. (14).

(4) Calculate the convection of each vortex element from Eq. (13).

(5) Calculate ω from Eq. (15).

(6) Calculate ψ from Eq. (12).

(7) Calculate ϕ from Eq. (11).

(8) Calculate u_l from Eq. (9).

(9) Correct the vorticity, or calculate the corrected vorticity from the curl of u_l.

Simulation Conditions

A vortex ring is launched toward a bubble cluster at initial time $t^*=0$. The vortex ring at launch is expressed by imposing the vorticity ω_ϕ within the cross-section of the vortex core. This simulation imposes the distribution used by Stanway et al. [18] and Wee-Ghoniem [19]. The vorticity is given by

$$\omega_\phi=\frac{K}{\pi}\frac{\Gamma_0}{a^2}\exp\left[-K\left(\frac{s}{a}\right)^2\right] \quad (19)$$

where a is the core radius, s is the distance from the vortex core, Γ_0 is the circulation, and $K=2.24182^2/4$, as shown in Figure 2. The *z*-axis is parallel to the central axis of the vortex ring, and the *x*-*y* plane passes through the center of the vortex core. The distance between the vortex cores on the *y*-*z* plane is the diameter of the vortex ring D_0 at launch.

The computational domain consists of a hexahedral region of $4D_0$ x $4D_0$x $12D_0$, as depicted in Figure 3. The vortex ring is launched from position $z = D_0$. It convects in the *z*-direction by self-induced velocity, colliding with small bubbles arranged in a hexahedral region of 3.2 D_0 x $3.2D_0$ x D_0. At the lateral boundaries $x = \pm 2D_0$ and $y = \pm 2D_0$ bottom boundary z = 0, a slip condition is imposed. At the upper boundary $z = 12D_0$, the velocity gradient is set at zero. The gravitational effect is ignored to investigate the interaction between the vorticity field around the vortex ring and bubble cluster.

The liquid-phase is water, whereas the gas-phase is hydrogen. The vortex core diameter $2a/D_0$ is set at 0.4. The Reynolds number of the vortex ring Γ_0/ν_0 ranges from 400 to 600. The bubble diameter d is 0.2 mm. The gas volume fraction at, $t^* = 0$, α_{g0} is set at 0.02 and 0.04. Table 1 lists the computational conditions.

The strength of the vortex ring or the circulation is calculated on the sections shown in Figure 4 by the equation as follows:

$$\Gamma=\frac{1}{4}\left(\int_{OPAB}\alpha_l\omega\cdot dS+\int_{OPCD}\alpha_l\omega\cdot dS+\int_{OPEF}\alpha_l\omega\cdot dS+\int_{OPGH}\alpha_l\omega\cdot dS\right) \quad (20)$$

where n is the unit vector normal to the plane.

The diameter D and displacement z_v of the vortex ring are measured

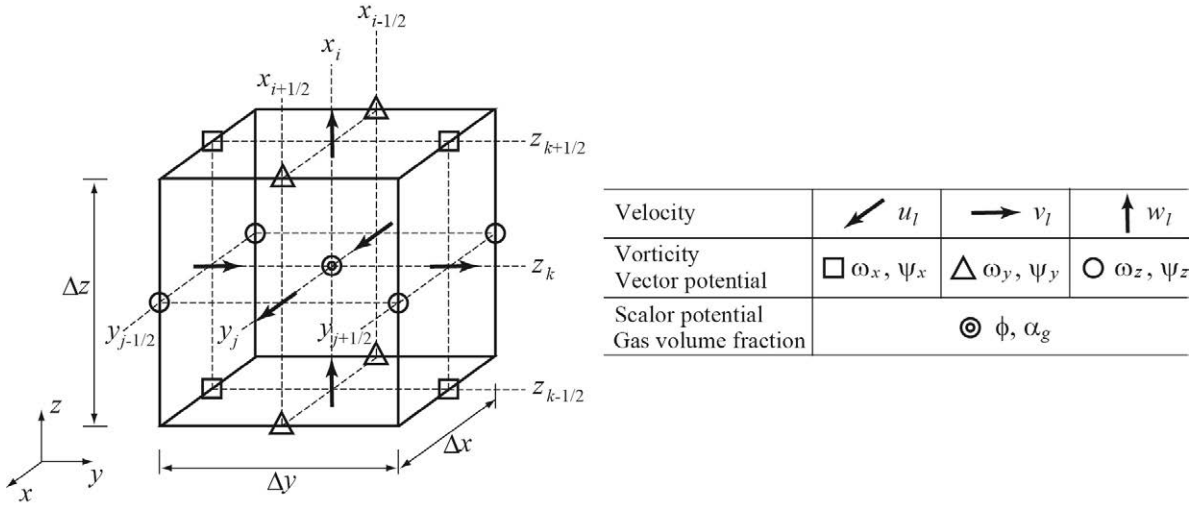

Figure 1: Staggered grid and computational variables.

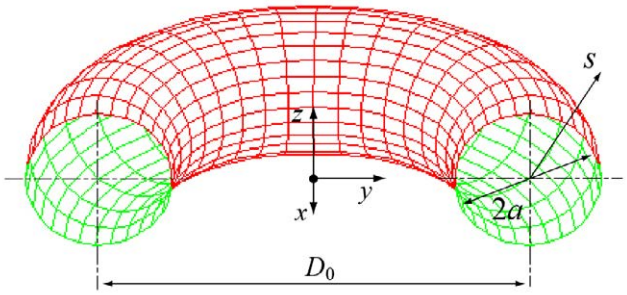

Figure 2: Vortex ring and coordinate system.

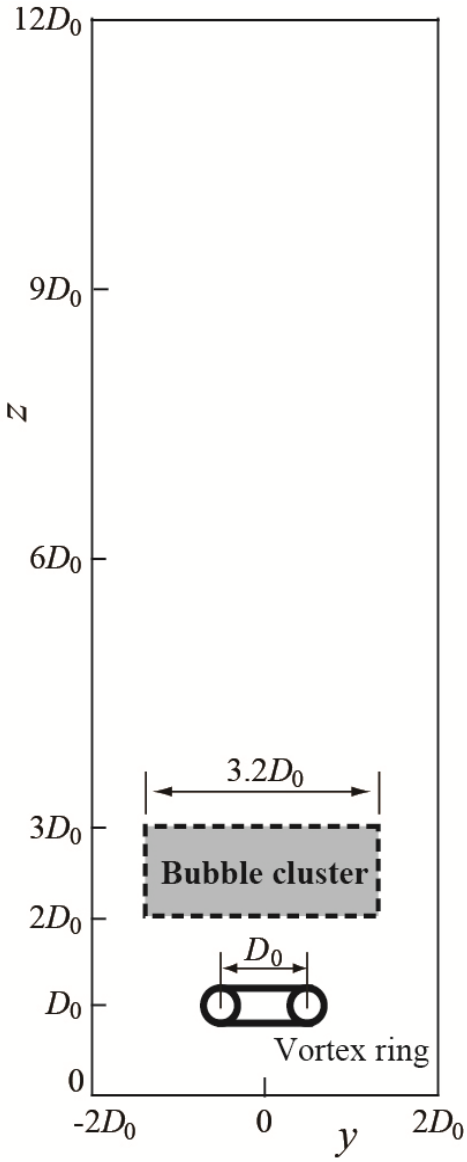

Figure 3: Computational domain and initial configuration of vortex ring and bubble cluster.

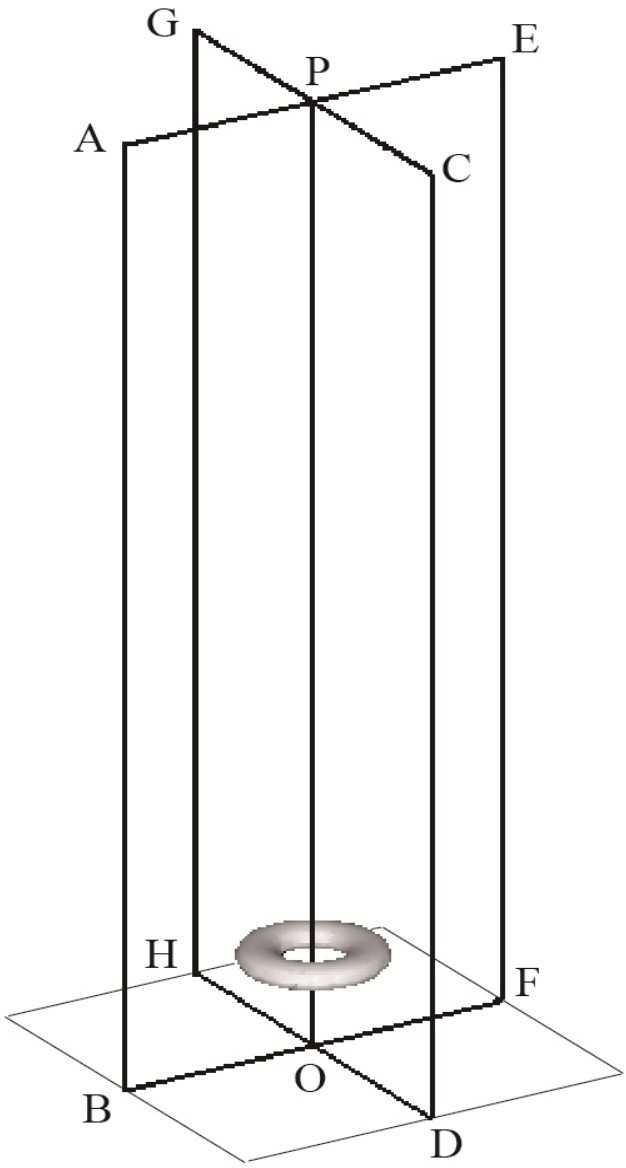

Figure 4: Vortex ring and control planes.

Gas/Liquid	Hydrogen/Water
Initial diameter of vortex ring; D_0 [mm]	42.5
Initial core diameter of vortex ring; $2a / D_0$	0.4
Reynolds number; $\mathrm{Re} = \Gamma_0 / \nu_l$	400,500,600
Computational domain	$4D_0 \times 4D_0 \times 12D_0$
Number of grids	48 × 48×144
Bubble diameter; d [mm]	0.2
Gas volume fraction of bubble cluster; α_{g0}	0, 0.02, 0.04
Lift coefficient of bubble; C_L	0.5
Virtual mass coefficient of bubble; C_V	0.5
Time increment; $\Gamma_0 \Delta t / D_0^2$	0.12

Table 1: Simulation conditions.

as shown in Figure 5 (a). To evaluate the entrainment and transport of the bubbles by the vortex ring, a control volume is set around the vortex ring, allowing the volume of the bubbles V_b in the control volume to be computed. Figure 5 (b) shows the cylindrical shape of the control volume. The diameter and height are $2D_0$ and $1.5D_0$, respectively, and the center coincides with the center of the vortex ring.

Results and Discussions

Behaviors of the vortex ring and bubble motion

The bubble distributions at four time points are presented in Figure 6. The Reynolds number Re is 500, and the bubble volume fraction at $t^* = 0$, α_{g0}, is 0.02. The vortex ring is visualized by an iso-surface for the second invariant of the velocity gradient tensor *Q*. The vortex ring, placed below the bubble cluster at $t^* = 0$, passes through the bubble cluster. At $t^* = 19.2$, it reaches a location separated by a distance of $2.3D_0$ from the upper side of the bubble cluster. The bubbles are distributed along the central axis of the vortex ring. The bubble entrainment by the vortex ring is captured. At the top of the vortex ring, the bubble involvement along the vortex core is also simulated. When $t^* = 38.4$, the entrainment and involvement continue, and the bubbles are distributed around all parts of the vortex ring. However, the number of bubbles near the central axis reduces, demonstrating the termination of the bubble entrainment. At $t^* = 82.8$, the bubbles are distributed on the surface of and inside a sphere surrounding the vortex ring, suggesting the transport of the bubbles by the vortex ring. The iso-surface of *Q* disappears because of the reduction of the strength of the vortex ring.

The vorticity distribution on a cross-section passing through the central axis of the vortex ring is shown in Figure 7 (a), where the bubbles in a slit region of thickness $0.047D_0$ are also plotted. The vortex ring convects through the bubble cluster, displacing the bubbles at t^* =4.8. When the vortex ring moves out of the bubble cluster at t^* =9.6, the bubbles are concentrated into thin layers, outlining the vortex core. The convection of the vortex ring entrains the bubbles along the central axis of the vortex ring (t^* =19.2), involving them in the vortex core (t^* =38.4). The entrained bubbles are transported by the vortex ring (t^* =82.8). The vorticity decreases with the passage of time. Figure 7 (b) shows the vorticity distribution laden with no bubbles. It is found that the bubble effect on the vorticity field is not very large.

Effect of initial bubble volume fraction α_{go}

The relation between the displacement z_v and convection velocity z_v of the vortex ring is shown in Figure 8, where Re=500. The velocity of $\alpha_{go} = 0.02$ is higher than that of $\alpha_{go} = 0$ at a displacement of $z_v/D_0 \leq 4.3$. As the density of the two-phase mixtures lowers, the fluid inertia also reduces, and therefore the reduction of the vorticity is relaxed. At $z_v/D_0 > 4.3$, however, the velocity of $\alpha_{g0} = 0.02$ decreases because the kinematic viscosity increases, in line with Eq. (3). This is also because the vorticity at $\alpha_{g0} = 0.02$ is lower than that at $\alpha_{g0} = 0$, as explained later.

Figures 8 and 9 shows the monotonously changing diameter of the vortex ring *D* with convection. At $z_v/D_0 > 4.3$, *D* is larger at higher α_{go} values, because the bubbles increase the viscosity and therefore reduce the vorticity around the vortex core.

Figure 10 shows the relation between the bubble volume around the vortex ring V_b and the displacement of the vortex ring z_v, where Re=500. When $\alpha_{go} = 0.02$, the volume V_b increases markedly immediately after the launch of the vortex ring. It reaches its maximum value at $z_v/D_0 = 3$ but falls rapidly with the convection of the vortex ring. The volume V_b is close to constant at $z_v/D_0 \geq 4.3$, suggesting that the entrained bubbles convect with the vortex ring. When $\alpha_{go} = 0.04$, V_b increases. The change against the displacement z_V is not affected by the α_{go} value.

The water velocity distribution across the central vertical cross-section of the vortex ring at Re=500 and $\alpha_{go} = 0.02$ is shown in Figure 11. The bubbles in a slit region of thickness $0.047D_0$ are plotted with the control volume. The distribution at the displacements of the vortex ring indicated by (a) - (f) in Figure 10 is shown. A marked increase in the bubble volume around the vortex ring immediately after the launch of the vortex ring can be seen at displacements (a) and (b). The vortex ring then convects through the bubble cluster. A decrease in the bubble volume occurs at displacements (c), (d) and (e). The bubbles are entrained and involved in the vortex ring. The bubble volume remains constant at displacement (f). The bubbles distribute themselves inside the vortex core and convect with the vortex ring.

The circulation of the vortex ring Γ changes as a function of z_v, as shown in Figure 12, where (a) - (f) indicate the displacements presented in Figure 11. When no bubbles are laden ($\alpha_{go} = 0$), Γ decreases monotonously with the convection of the vortex ring. The Γ value for $\alpha go = 0.02$ is larger than that for $\alpha_{go} = 0$ at $z_v/D_0 \leq 5.7$. This is caused by the fact that the falling density of the two-phase mixtures, which reduces the inertia of the fluid, lowers the reduction of the vorticity. At displacement (f), Γ for the bubble-laden condition is lower than that for $\alpha_{go} = 0$ because the bubbles are distributed in a thin layer inside the vortex ring and because the vorticity is markedly low. The change in Γ at $\alpha_{go} = 0.04$ is larger than that at $\alpha_{go} = 0.02$.

Effect of Reynolds number

The time variation of the displacement of the vortex ring is shown in Figure 13. The effect of the bubbles strengthens as Re decreases. The vortex ring decelerates markedly after passing through the bubble cluster.

Figure 14 shows Γ decreasing in line with the decrease in Re, confirming the reduction of the convection velocity of the vortex ring shown in Figure 13.

The bubble volume around the vortex ring against the displacement of the vortex ring is shown in Figure 15. The volume is higher for lower Re values at $z_v/D_0 \geq 4.3$ because the slower convection means that the vortex ring remains in the bubble cluster for longer time, and therefore more bubbles are entrained. The convection velocity and circulation of the vortex ring fall at lower Re values as shown in Figures 13 and 14. It is found that the reduction reflects the increased bubble volume around the vortex ring.

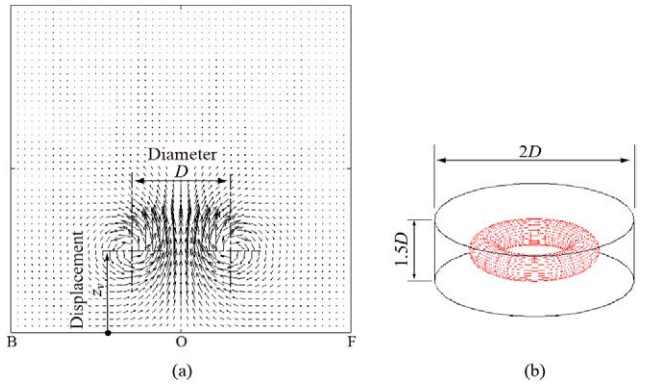

Figure 5: Displacement Z_v, diameter *D*, and control volume of vortex ring.

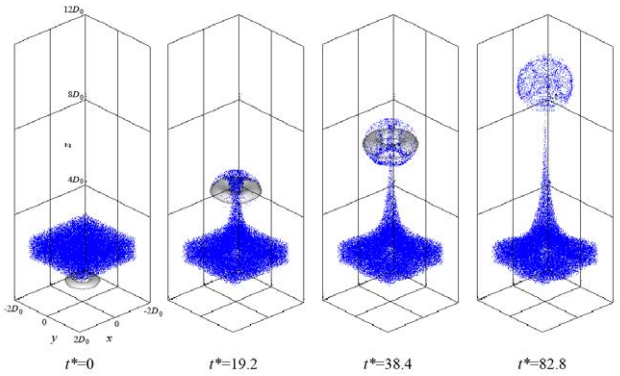

Figure 6: Temporal evolution of bubble distribution and vortex ring expressed by iso-surface of $Q/\left(D_0^4/\Gamma_0^2\right)=0.01$.

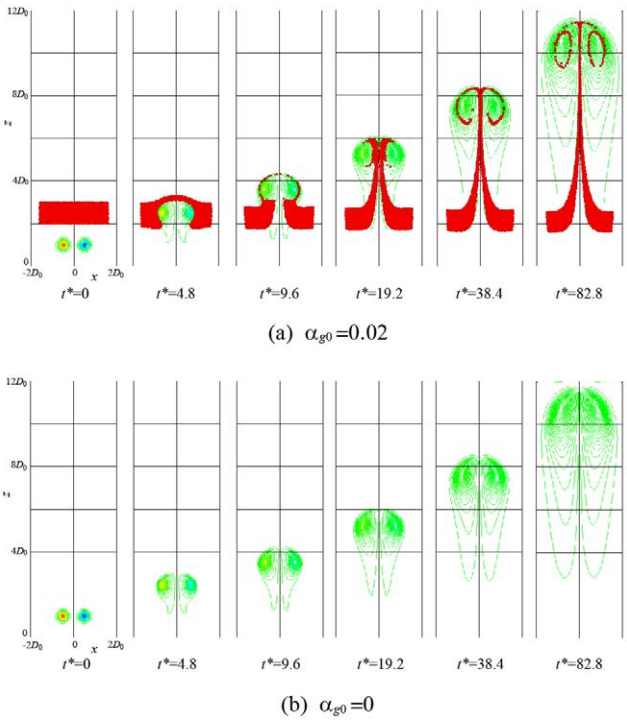

Figure 7: Temporal evolution for 2D distribution of vorticity and bubble.

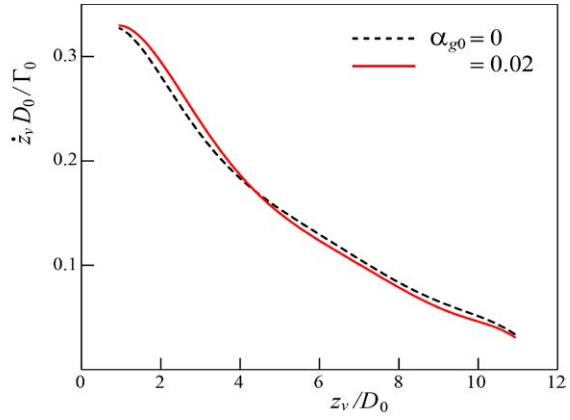

Figure 8: Change in convection velocity of vortex ring.

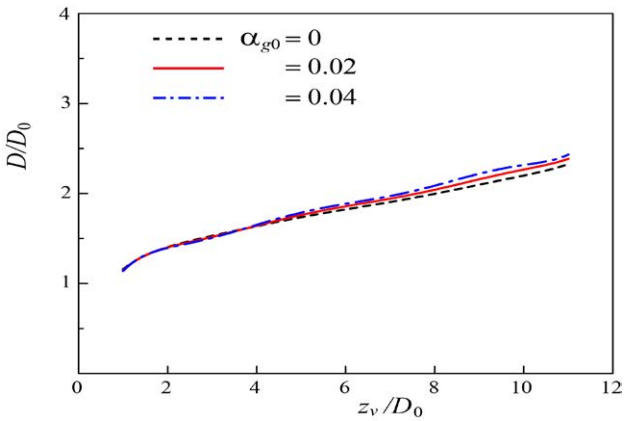

Figure 9: Change in diameter of vortex ring.

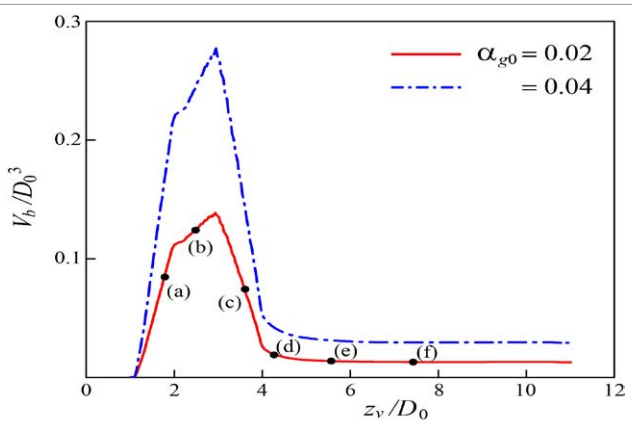

Figure 10: Change in bubble volume around vortex ring.

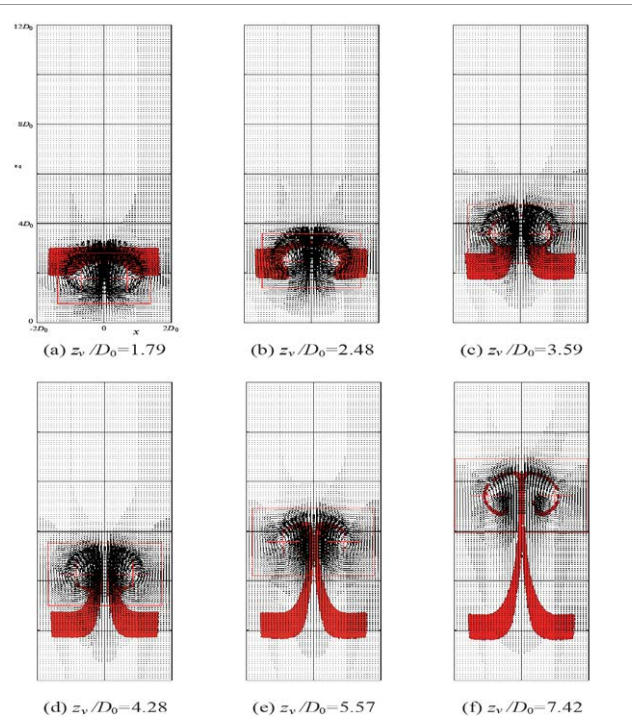

Figure 11: Temporal evolution for 2D distributions of water velocity and bubble.

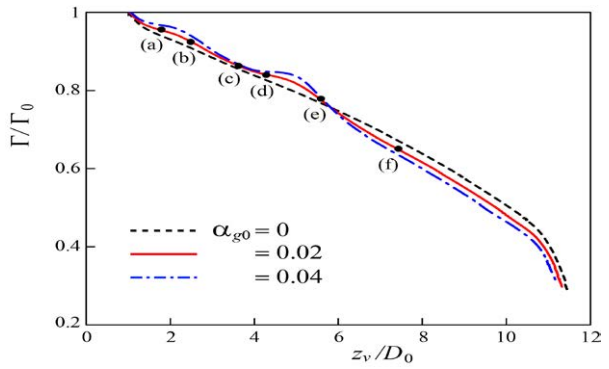

Figure 12: Change in circulation with convection of vortex ring.

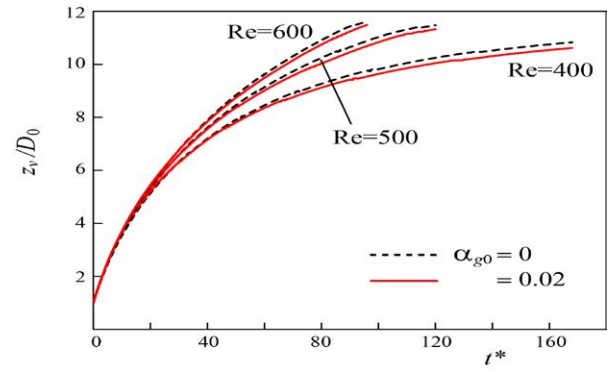

Figure 13: Effect of Reynolds number on displacement of vortex ring.

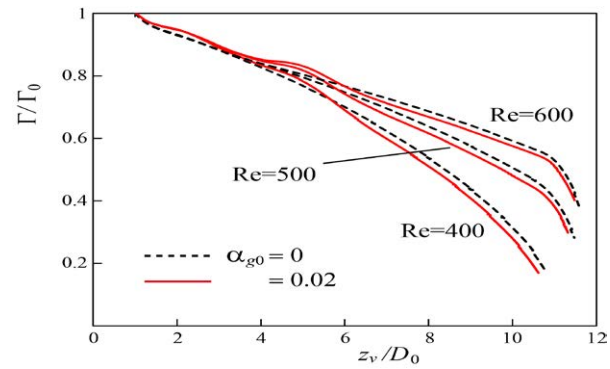

Figure 14: Effect of Reynolds number on circulation.

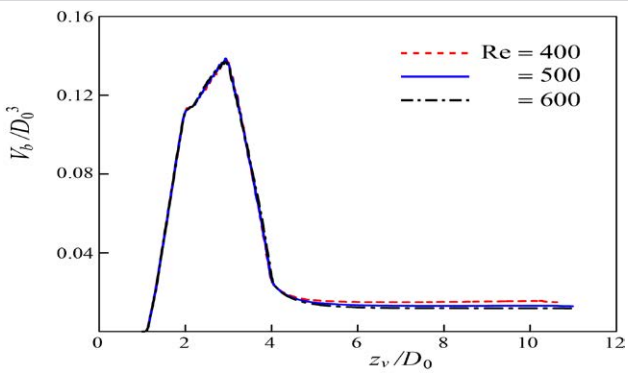

Figure 15: Effect of Reynolds number on bubble volume around vortex ring.

Conclusions

The control of the motion of small gas bubbles by a vortex ring is explored through numerical simulation. Hydrogen bubbles with a diameter of 0.2 mm are arranged in quiescent water, and a vortex ring is launched toward the bubbles. The behaviors of the vortex ring and bubble motion are analyzed by the VIC method developed by the authors. The diameter of the vortex ring at launch D_0 is 42.5 mm and the bubble volume fraction at launch α_{go} is less than 0.04. The results are summarized as follows:

(1) The vortex ring convects through the bubble cluster, displacing and entraining the bubbles. After passing through the cluster, the bubbles are involved in the vortex core. The volume of the bubbles transported by the vortex ring remains unaltered when the displacement of the vortex ring z_v is larger than $7D_0$.

(2) The convection velocity of the vortex ring at αgo = 0.02 is higher than that at $\alpha_{go} = 0$ with a displacement of $z_v /D_0 \leq 4.3$. This is caused by the fact that the falling density of the two-phase mixtures, which reduces the inertia of the fluid, lowers the reduction of the vorticity. However, the velocity falls at $z_v /D_0 > 4.3$. This is attributable to the increase in viscous diffusion, and also because of the reduction of the vorticity.

(3) The diameter of the vortex ring increases with convection. The increment becomes greater as α_{go} increases.

(4) The volume of bubbles transported by the vortex ring is larger at lower Re values, reflecting the fall in the convection velocity of the vortex ring.α_{go}

Reference

1. Rightley PM, Lasheras JC (2000) Bubble dispersion and interphase coupling in a free-shear flow. Journal Fluid Mechanics 412: 21-59.
2. Aliseda A, Lasheras JC (2006) Effect of buoyancy on the dynamics of a turbulent boundary layer laden with microbubbles. Journal of Fluid Mechanics 559: 307-334.
3. Balachandar S, Eaton JK (2010) Turbulent dispersed multiphase flow. Ann. Rev. Fluid Mech 42: 111-133.
4. Abe Y, Kawaji M, Watanabe T (2002) Study on the bubble motion control by ultrasonic wave. Exp Thermal and Fluid Sci 26: 817-826.
5. Cui A, Li Y, Ge Y, Fan LS (2005) Bubble modulation using acoustic standing waves in a bubbling system. Chem. Eng. Sci 60: 5971-5981.
6. Kurokawa J, Ohtaki T (1995) Gas-liquid flow characteristics and gas-separation efficiency in a cyclone separator. Proc. ASME/JSME Fluids Engineering and Laser Anemometry Conference and Exhibition. FED 225: 51-57.
7. Movafaghian S, Jaua-Marturet JA, Mohan RS, Shoham O, Kouba GE (2000) The effects of geometry, fluid properties and pressure on the hydrodynamics of gas-liquid cylindrical cyclone separators. Int. J. Multiphase Flow 26: 999-1018.
8. Ruetsch GR, Meiburg E (1994) Two-way coupling in shear layers with dilute bubble concentrations. Phys. Fluids 6: 2656-2670.
9. Druzhinin OA, Elghobashi SE (2001) Direct numerical simulation of a three-dimensional spatially developing bubble-laden mixing layer with two-way coupling. J. Fluid Mech 429: 23-61.
10. Uchiyama T, Kusamich S (2013) Interaction of bubbles with vortex ring launched into bubble plume. Advances in Chemical Engineering and Science 3: 207-217.
11. Sridhar G, Katz J (1995) Drag and lift forces on microscopic bubbles entrained by a vortex. Phys. Fluids 7: 389-399.
12. Sridhar G, Katz J (1999) Effect of entrained bubbles on the structure of vortex rings. J. Fluid Mech 397: 171-202.
13. Uchiyama T, Yoshii Y, Hamada H (2014) Direct numerical simulation of a turbulent channel flow by an improved vortex in cell method. Int. J. Numerical Methods for Heat and Fluid Flow 24: 103-123.

14. Uchiyama T, Yoshii Y, Chen B, Wang Z (2015) Numerical simulation of bubbly flow by an improved vortex in cell method. Advances and Applications in Fluid Mechanics 17: 91-114.

15. Uchiyama T, Kishimoto Y (2014) Numerical simulation of air-water bubbly jet issuing from a square nozzle by a vortex in cell method. Chem. Eng. Process Technol 5: 207.

16. Taylor GI (1932) The viscosity of a fluid containing small drops and another fluid. Proc. R. Soc. Lond. A 138: 41-48.

17. Cottet GH, Koumoutsakos PD (2000) Vortex Methods: Theory and Practice. Cambridge University Press.

18. Stanaway SK, Cantwell BJ, Spalart PR (1988) A numerical study of viscous vortex rings using a spectral method. NASA TM-101041.

19. Wee D, Ghoniem AF (2006) Modified interpolation kernels for treating diffusion and remeshing in vortex methods. J. Comput. Phys 213: 239-263.